Optimal Strength Design for Fiber–Metal Laminates and Fiber-reinforced Plastic Laminates

WENJIE PENG,[1,2,3] JIANQIAO CHEN,[2,3,*] JUNHONG WEI[2,3] AND WENQIONG TU[2,3]

[1]*Research and Development Center, Wuhan Iron and Steel (Group) Corp Wuhan 430083, PR China*

[2]*Department of Mechanics, Huazhong University of Science and Technology Wuhan 430074, PR China*

[3]*Hubei Key Laboratory for Engineering Structural Analysis and Safety Assessment Wuhan 430074, PR China*

ABSTRACT: Optimal strength design of fiber-reinforced plastic (FRP) laminates and fiber–metal laminates (FML) is studied in this article. An optimization approach that integrates the particle swarm optimization algorithm and a general finite element code ANSYS was developed. ANSYS is utilized to obtain the failure index as fitness function and the optimum fitness is obtained by altering the fiber orientations. The strength behavior of FRP and FML under in-plane load and out-of-plane load is compared based on the optimization results. Results show that for in-plane load, due to the substituting of metal alloy sheet for prepreg layer, the strength behavior in transverse direction is enhanced and FML has better resistance to biaxial load. For out-of-plane point load, FML offers strength performance superior to that of FRP and is more stable for all the boundary conditions investigated.

KEY WORDS: fiber–metal laminates, FEM, particle swarm optimization, optimal strength design.

INTRODUCTION

FIBER–METAL LAMINATE (FML) is a new class of composite material for advanced aerospace/aeronautical structural applications arisen in the recent years. It consists of thin aluminum alloy sheets bonded together with fiber-reinforced epoxy prepreg. These laminates demonstrate advantages over conventional monolithic aluminum alloys or fiber-reinforced plastic (FRP) composite materials, such as excellent impact properties [1–3], fire and corrosion behavior [4,5], and fatigue properties [6,7]. In addition, FML retains the conventional workshop practices of metals, namely, easy machining, forming, and

*Author to whom correspondence should be addressed. E-mail: jqchen@mail.hust.edu.cn

0021-9983/11/02 0237–18 $10.00/0 DOI: 10.1177/0021998310373521

mechanical fastening abilities [8]. These advantages facilitate the use of FML for primary structures in aerospace industry.

Until now, there are commercial products under the labels GLARE^{TM} and ARALL^{TM}. The fiber orientations in these commercial laminates are stacked in fixed direction. In fact, FML can also be designed to meet specific requirements by varying the stacking sequence of fiber prepreg as FRP. However, most studies in literature about FML dealt with the analysis or experimental test of mechanical properties of FML [1–9], but few studies dealt with the optimization of FML. The literature concerning with optimization of composite structures are mainly concentrated on the strength design of FRP [10–17]. In these literatures, the structure analysis of FRP is done by either finite element method (FEM) [10–13] or classical lamination theory (CLT) [14–17] and the failure index (FI) evaluated based on failure criteria is taken as the objective function [10,11,17] or the constraint function [12–17].

Considering the elastic–plastic behavior of metal layers in FML, CLT is first modified and extended to be applicable to nonlinear cases. Although CLT is capable of predicting in-plane stresses and strains, CLT assumes that the laminates are of plane stress condition and the out-of-plane stress components are neglected. Consequently, for out-of-plane load, CLT will lead to solutions with large inaccuracy and it is difficult to deal with complex boundary conditions. Therefore, a general finite element (FE) code ANSYS is utilized to perform the structure analysis of laminates under different loads and boundary conditions in this study.

In this study, optimal strength design of FRP laminates and FML under in-plane load and out-of-plane load is conducted. An out-of-plane point force is loaded at the top center of a laminate to model an impact loading approximately [18–20]. The failure indices are obtained through Tsai–Wu criterion for FRP layers and Von Mises criterion for metal layers. The maximum and minimum failure indices of FRP and FML are calculated respectively via altering the fiber orientations of prepreg layers. As the optimization methods included in ANSYS have the disadvantage of being sensitive to initial designs, a technique of applying an exterior evolutional optimization algorithm particle swarm optimization (PSO) integrated with ANSYS was developed for optimization. Based upon the optimization results, the strength behaviors of FML and FRP are discussed and compared and the superiority of FML is demonstrated.

MODIFIED AND EXTENDED CLT

Modified Classical Lamination Theory for FML

Traditional CLT is used to analyze the displacement, in-plane stresses, and strains of FRP. With CLT, plane stress condition is assumed for each ply and out-of-plane stress components are neglected.

Figure 1 is a typical FML. With respect to the coordinate system shown in Figure 2, due to compatibility of the layers in FML, all layers experience the same deformations. For FML subjected to in-plane load, the in-plane stress components of the FRP layer in the principal material axes are related to the strain components as:

$$\begin{Bmatrix} \sigma_1 \\ \sigma_2 \\ \tau_{12} \end{Bmatrix} = \begin{bmatrix} Q_{11} & Q_{12} & 0 \\ Q_{12} & Q_{22} & 0 \\ 0 & 0 & Q_{66} \end{bmatrix} \begin{Bmatrix} \varepsilon_1 \\ \varepsilon_2 \\ \gamma_{12} \end{Bmatrix}, \tag{1}$$

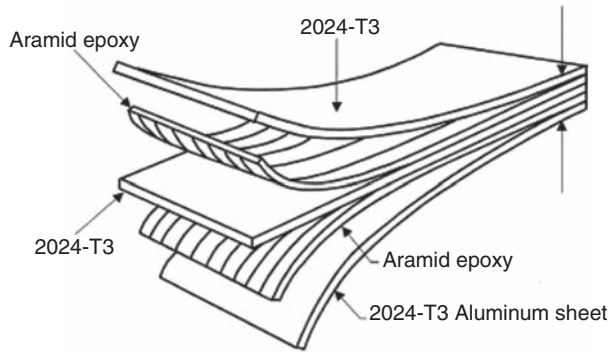

Figure 1. *A scheme of FML.*

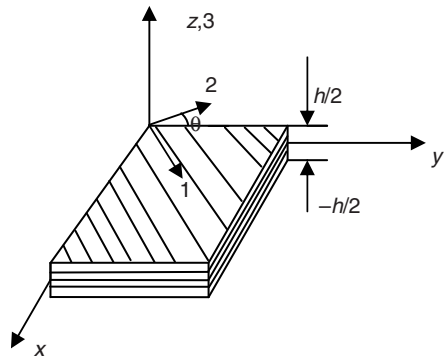

Figure 2. *A scheme of coordinate system.*

where Q_{ij} are the principal stiffness components:

$$Q_{11} = \frac{E_1}{1-\mu_{12}\mu_{21}},\ Q_{22} = \frac{E_2}{1-\mu_{12}\mu_{21}},\ Q_{66} = G_{12},\ Q_{12} = \mu_{12}Q_{22} = \mu_{21}Q_{11}. \tag{2}$$

Transforming the stress components in the principal material axes to the reference coordinate axes, the stress components of an arbitrary layer are expressed as:

$$\begin{Bmatrix} \sigma_x \\ \sigma_y \\ \tau_{xy} \end{Bmatrix}_k = \begin{bmatrix} \overline{Q}_{11} & \overline{Q}_{12} & \overline{Q}_{16} \\ & \overline{Q}_{22} & \overline{Q}_{26} \\ \text{sym.} & & \overline{Q}_{66} \end{bmatrix}_k \begin{Bmatrix} \varepsilon_x \\ \varepsilon_y \\ \gamma_{xy} \end{Bmatrix}_k, \quad \begin{Bmatrix} \varepsilon_x \\ \varepsilon_y \\ \gamma_{xy} \end{Bmatrix}_k = \begin{bmatrix} \varepsilon_x^0 \\ \varepsilon_y^0 \\ \gamma_{xy}^0 \end{bmatrix} + z \begin{bmatrix} K_x \\ K_y \\ K_{xy} \end{bmatrix}, \tag{3}$$

where k is the lamina number counted from the bottom and $\overline{Q}_{ij}$ the off-axis stiffness components, which can be expressed in terms of Q_{ij} [21]. $\varepsilon_x^0, \ldots$ are mid-plane strains, and $K_x, \ldots$ the mid-plane curvatures.

The constitutive equation of the metal layer is:

$$\begin{Bmatrix} \sigma_x \\ \sigma_y \\ \tau_{xy} \end{Bmatrix} = \begin{bmatrix} Q_{11,m} & Q_{12,m} & Q_{16,m} \\ & Q_{22,m} & Q_{26,m} \\ \text{sym.} & & Q_{66,m} \end{bmatrix} \begin{Bmatrix} \varepsilon_x \\ \varepsilon_y \\ \gamma_{xy} \end{Bmatrix}, \tag{4}$$

where $Q_{ij,m}$ are the stiffness components of the metal layer. For homogenized linear elastic isotropic material under plane stress assumption, the stress–strain relation is:

$$Q_{11,m} = Q_{22,m} = \frac{E}{(1-\mu^2)}; \quad Q_{12,m} = E\frac{\mu}{(1-\mu^2)}; \quad Q_{66,m} = \frac{E}{2(1+\mu)}; \quad Q_{16,m} = Q_{26,m} = 0. \tag{5}$$

Integrating the stresses of FRP layers and metal layers, that is, Equations (3) and (4) with respect to the z-direction, we obtain the resultant forces and moments as:

$$\begin{pmatrix} \mathbf{N} \\ \mathbf{M} \end{pmatrix} = \begin{bmatrix} \mathbf{A} & \mathbf{B} \\ \mathbf{B} & \mathbf{D} \end{bmatrix} \begin{pmatrix} \boldsymbol{\varepsilon_0} \\ \boldsymbol{\kappa} \end{pmatrix}, \tag{6}$$

$$\begin{pmatrix} \boldsymbol{\varepsilon_0} \\ \boldsymbol{\kappa} \end{pmatrix} = \begin{bmatrix} \mathbf{a} & \mathbf{b} \\ \mathbf{b} & \mathbf{d} \end{bmatrix} \begin{pmatrix} \mathbf{N} \\ \mathbf{M} \end{pmatrix}, \tag{7}$$

where

$$\begin{aligned} A_{ij} &= \sum_{k=1}^{n_f} (\bar{Q}_{ij,f})_k (h_k - h_{k-1}) + \sum_{l=1}^{n_m} (Q_{ij,m})_l (h_l - h_{l-1}), \ i,j = 1,2,6 \\ B_{ij} &= \frac{1}{2}\left[\sum_{k=1}^{n_f} (\bar{Q}_{ij,f})_k (h_k^2 - h_{k-1}^2) + \sum_{l=1}^{n_m} (Q_{ij,m})_l (h_l^2 - h_{l-1}^2)\right], \ i,j = 1,2,6. \\ D_{ij} &= \frac{1}{3}\left[\sum_{k=1}^{n_f} (\bar{Q}_{ij,f})_k (h_k^3 - h_{k-1}^3) + \sum_{l=1}^{n_m} (Q_{ij,m})_l (h_l^3 - h_{l-1}^3)\right], \ i,j = 1,2,6 \end{aligned} \tag{8}$$

A_{ij}, B_{ij}, and D_{ij} are the components of extensional, coupling, and bending stiffness matrices; a_{ij}, b_{ij}, and d_{ij} the corresponding compliance matrices; n_f and $n_{m,}$ the number of FRP layers and metal layers, respectively; and h the coordination in z-direction defined as Figure 3. **N**, **M** are the forces and moments per unit length of the cross-section, respectively.

Giving the load **N** and M, the strain components $\boldsymbol{\varepsilon_0}$ and $\boldsymbol{\kappa}$ can be obtained through Equation (7). Substituting ε_0 and κ into Equations (3) and (4), the stress components of

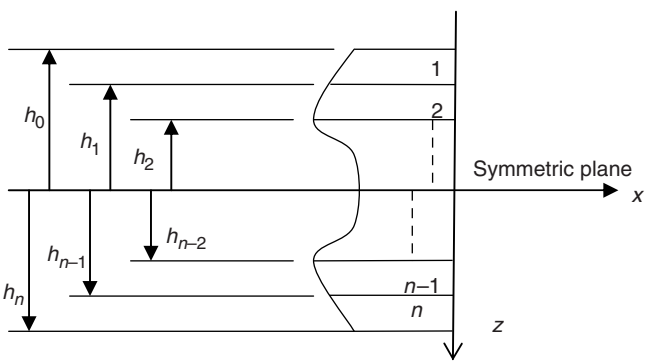

Figure 3. *The definition of h_k in the coordination.*

FRP layers and metal layers in the reference coordinate axes can be obtained. The principal stress components of FRP are then solved using the following transformation:

$$\begin{Bmatrix} \sigma_1 \\ \sigma_2 \\ \tau_{12} \end{Bmatrix}_k = \begin{bmatrix} m^2 & n^2 & 2mn \\ n^2 & m^2 & -2mn \\ -mn & mn & m^2 - n^2 \end{bmatrix} \begin{Bmatrix} \sigma_x \\ \sigma_y \\ \tau_{xy} \end{Bmatrix}_k, \; m = \cos\theta, \; n = \sin\theta \tag{9}$$

Elasto-plastic Behavior of FML

The above modified classical lamination theory (MCLT) involves linear elasticity, and the elastic–plastic behavior of metal layers was not considered. Some researchers [9,22] used the flow theory of Von Mises type to describe the elasto-plastic behavior of aluminum alloy. In this article, a simple bi-linear laws method is adopted to model the nonlinear behavior of metal layer as shown in Figure 4. Von Mises criterion was used to predict the yielding of metal. When the equivalent stress of the metal layer reaches the yield strength, the modulus decreases from E_e to E_p. Given the failure strength and ultimate strain, the Young's modulus after yielding can be calculated as follows:

$$E_p = \frac{\sigma_{ult} - \sigma_y}{\varepsilon_{ult} - \sigma_y / E_e}, \tag{10}$$

where σ_{ult} and σ_y are the failure strength and the yielding strength of metal layer, respectively, and ε_{ult} is the ultimate strain.

Using bi-linear laws, the laminate constitutive equation can be expressed in incremental form and E in Equation (5) is taken as follows:

$$\begin{aligned} &E = E_e \text{ for } \sigma_{eq} < \sigma_y, \text{ or } \sigma_{eq} > \sigma_y \text{ and } dN < 0. \\ &E = E_p \text{ for } \sigma_{eq} > \sigma_y \text{ and } dN > 0. \end{aligned} \tag{11}$$

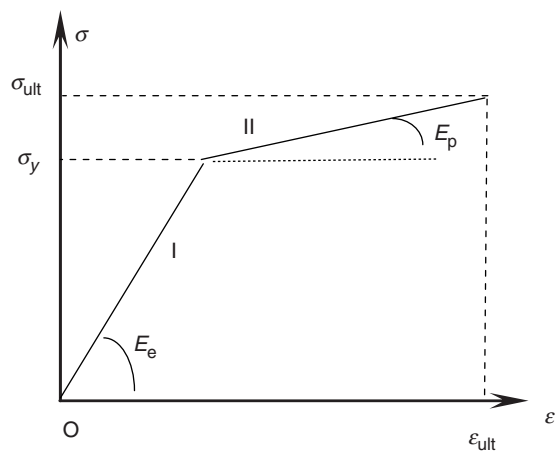

Figure 4. *The bi-linear stress–strain curve of metal layer.*

Numerical Analysis and MCLT Prediction of Stresses in FML Under In-plane Tensile Load

In this section, FE modeling is performed with ANSYS and the tensile behavior of FML is simulated. Numerical simulation results are compared with the analytical predictions by MCLT. The laminate for calculation is of stacking sequence of [Al/45°/−45°/Al/Al/−45°/45°/Al] under uniaxial in-plane load $N_x = 10\,\text{N/mm}$, where 'Al' indicates aluminum sheet, and 45° or −45° represents the angle between the fiber direction and the x-direction. The material of aluminum sheet is 2024-T3, $E = 76\,\text{GPa}$, $v = 0.34$. The FRP layers were modeled with homogenized linear elastic orthotropic material with material properties listed in Table 1. Each layer is 0.125 mm in thickness.

Quarter of the laminate was modeled due to symmetry of stacking sequence and load. As the gradient of stresses at the free edge is large, it is essential to refine mesh at these regions. The predicted stresses obtained by MCLT are listed in Table 2. The predicted stress distribution of FRP layer and Al layer along the width (y-direction) by ANSYS are plotted in Figures 5 and 6 and the strains are $\varepsilon_x = 2.05\text{e}{-4}$, and $\varepsilon_y = -1.0\text{e}{-4}$. It is shown that the predicted stresses and strains from ANSYS and MCLT show good agreements except for the edge region. ANSYS characterizes the local peak stresses at the free edge in detail, which are not regarded by MCLT.

Table 1. Material properties for FRP layer (T300/5308).

E_1 (GPa)	E_2, E_3 (Gpa)	G_{12}, G_{13} (GPa)	G_{23} (GPa)	μ_{12}, μ_{23}, μ_{13}
135	8.0	4.5	3.97	0.34

Table 2. Predicted stresses and strains under uniaxial tensile load by MCLT.

Layers of FML	σ_x (MPa)	σ_y (MPa)	τ_{xy} (MPa)	ε_x	ε_y
2024-T3	14.695	–2.57	0		
45°	5.305	2.56	3.37	2.05E–04	–1.0E–05
−45°	5.305	2.56	–3.37		

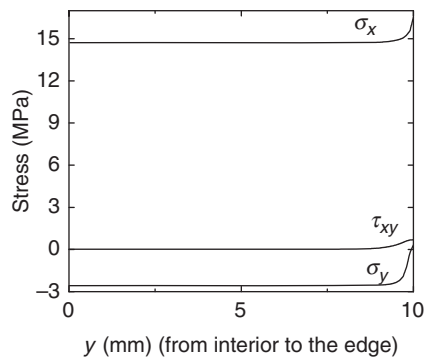

Figure 5. *Stress distribution in Al layer (x is the loading direction).*

Modeling of Tensile Tests

In order to validate the numerical and analytical predictions further, ANSYS and MCLT are utilized respectively to model the tensile test of FML and validated with the experimental results in literature [22]. The FML for tensile test is GLARE 5-1/2 of which the stacking sequence is [Al/0/90°/90°/0/Al]. It is of straight rectangular geometry with length = 305 mm and width = 25.5 mm. The thickness is 0.489 mm for each Al layer and 0.146 mm for each prepreg layer. The mechanical properties of the constituents of GLARE 5-1/2 are listed in Table 3. The fiber volume fraction in the prepreg layer was 50%; thus, the mechanical properties of the prepreg layer can be calculated using the mixture rule [21], listed in the last line of Table 3.

When modeling with ANSYS, uniaxial monotonously deformation is applied in the longitudinal direction. The tensile stress–strain curves of GLARE 5-1/2 are plotted in Figure 7.

From Figure 7, it is observed that due to the bi-linear stress–strain relationship of Al layers as well as linear elastic behavior of FRP, FML also exhibited bi-linear stress–strain behavior under tensile load. The initial longitudinal modulus of FML was found to be 55 GPa. Subsequently, at a stress level of 267 MPa, Al layer starts yielding and the longitudinal modulus of FML decreases to 10.2 GPa. After yielding, the load-carrying capability of Al decreases substantially. As a result, the stresses in the Al layer are redistributed among the prepreg layers. As the applied deformation increases continuously, failure modes such as matrix cracking, fiber breaking, and debonding of fiber–epoxy

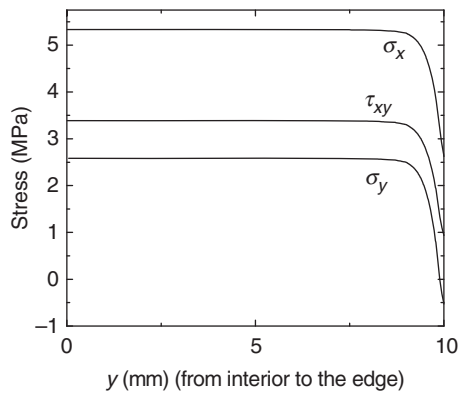

Figure 6. *Stress distribution in 45° layer (x is the loading direction).*

Table 3. The mechanical properties of the constituents of GLARE 5-1/2.

Materials	E_1 (GPa)	E_2 (GPa)	G_{12} (GPa)	σ_y (MPa)	$E_{plastic}$ (MPa)	μ_{12}
2024-T3	72	72	26.6	350	887	0.33
Glass fiber	86	86	32.3	–	–	0.33
Epoxy	3.4	3.4	1.26	–	–	0.35
GFRP	44.7	6.54	2.43	–	–	0.34

Note: GFRP, glass fiber-reinforced plastic.

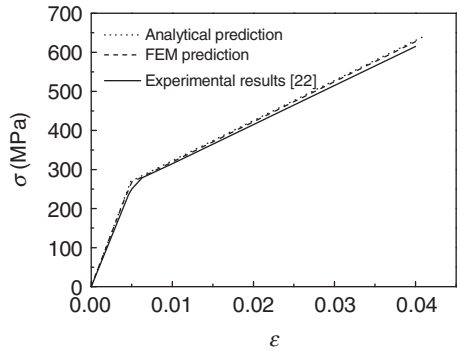

Figure 7. *Stress–strain curves of GLARE 5-1/2 under tensile load.*

will occur. These failure modes will lead to stiffness degrading of FRP; thus, at a higher stress level, the predictions by MCLT and ANSYS deviate from experimental results as the stiffness degrading was not considered. Nevertheless, the agreement between the prediction and the experiments is good as a whole, implying that both the FE analysis and the MCLT modeling can characterize the elastic or elastic–plastic properties of FML at a good level.

Failure Strength Prediction

In order to guarantee secure use of FML in aeronautical applications, it is assumed that FML failed when either the prepreg layer fails or the metal layer yields. The corresponding failure strength is regarded as first ply failure (FPF) threshold. The Tsai–Wu [23,24] criterion is used to predict the failure of prepreg layer for it can account for interactions between the different stress components, and Von Mises criterion is used for metal layer. The failure criterion of FML can be expressed as follows:

$$\max[f(\theta_{\mathrm{f}}), f(\theta_{\mathrm{m}})] = 1, \tag{12}$$

where $f(\theta_{\mathrm{f}})$ denotes the FI of prepreg layer. A small value of FI stands for a safer condition. For an orthotropic ply under 3D stress condition, its FI corresponding to Tsai–Wu [23] criterion is:

$$\begin{aligned} f(\theta_f) = {} & F_{11}\sigma_1^2 + F_{22}\sigma_2^2 + F_{33}\sigma_3^2 + 2F_{12}\sigma_1\sigma_2 + 2F_{23}\sigma_2\sigma_3 \\ & + 2F_{13}\sigma_1\sigma_3 + F_{44}\tau_{12}^2 + F_{55}\tau_{23}^2 + F_{66}\tau_{13}^2 + F_1\sigma_1 + F_2\sigma_2 + F_3\sigma_3, \end{aligned} \tag{13}$$

where

$$\begin{aligned} & F_{11} = 1/X_{\mathrm{T}}X_{\mathrm{C}}, F_{22} = 1/Y_{\mathrm{T}}Y_{\mathrm{C}}, F_{33} = 1/Z_{\mathrm{T}}Z_{\mathrm{C}}, \\ & F_{44} = 1/R^2, F_{55} = 1/S^2, F_{66} = 1/T^2, F_1 = \frac{1}{X_{\mathrm{T}}} - \frac{1}{X_{\mathrm{C}}}, F_2 = \frac{1}{Y_{\mathrm{T}}} - \frac{1}{Y_{\mathrm{C}}}, F_3 = \frac{1}{Z_{\mathrm{T}}} - \frac{1}{Z_{\mathrm{C}}}, \\ & F_{12} = -0.5\sqrt{F_{11}F_{22}}, F_{23} = -0.5\sqrt{F_{22}F_{33}}, F_{13} = -0.5\sqrt{F_{11}F_{33}}. \end{aligned} \tag{14}$$

X_{T} and X_{C} are the tensile and compressive strengths along the fiber direction respectively, Y_{T} and Y_{C} the tensile and compressive strengths along the transverse direction,

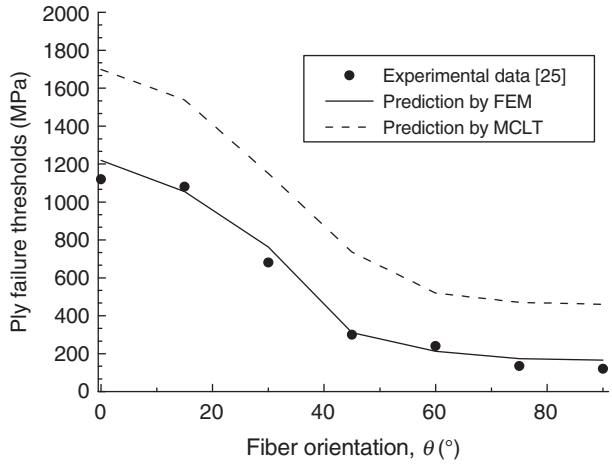

Figure 8. *A comparison of the FPF thresholds in titanium-based FML.*

respectively, R and T the out-of-plane shear strengths, and S the in-plane shear strength. $f(\theta_m)$ is the FI of the metal layer:

$$f(\theta_m) = (1/Y)\sqrt{\sigma_x^2 + \sigma_y^2 + \sigma_z^2 - (\sigma_x\sigma_y + \sigma_x\sigma_z + \sigma_y\sigma_z) + 3(\tau_{xy}^2 + \tau_{xz}^2 + \tau_{yz}^2)}, \qquad (15)$$

where Y is the yield strength.

For modeling yielding by FEA and CLT, the load is gradually increased, and when the FI of prepreg layer or metal layer reaches '1', the corresponding applied load is defined as FPF threshold. A comparison of the experimentally determined FPF thresholds [25] with the predictions by FEM and MCLT are shown in Figure 8.

The metal in the FML investigated in literature [25] was a titanium Ti–15V–3Cr–3Al–3Snβ alloy foil with high tensile failure strength. The stacking sequence is $[\mathrm{Ti}, \pm\theta^\circ]$s. Mechanical properties can be found in the literature. It is indicated that agreement of numerical prediction by FEA and experimental data is good over the range of the fiber orientations from 0° to 90° varied in 15° intervals. The prediction by MCLT, however, is higher than the actual one. In addition, it is observed that FPF threshold decreases rapidly with increasing θ. The failure threshold does not vary significantly for the angles greater than 45° as at angles of 45° and above, the tensile properties of the metal layers dominate the behavior of the FML. It can be seen that the tensile response by ANSYS correlates well with analytical and experimental results and the failure thresholds strongly depend on the fiber orientations. Since the failure is controlled by local peak stresses or weakest area. However, MCLT's basic hypothesis involves stress evenly distributed everywhere in each ply; thus, the local peak stresses are not considered. Moreover, MCLT assumes that the laminates are of plane stress condition and the through thickness stress components are neglected. Consequently, the strength behavior cannot be predicted as accurately as the elastic or elastic–plastic properties. Although MCLT does not give satisfactory results for the strength prediction, it can serve as a starting base for evaluating and optimizing the elastic properties of FML. As discussed earlier, FEM based on ANSYS is more sophisticated than MCLT in structure analysis of laminated composite for general cases. In this article, the FPF strength is focused.

The optimization method and numerical optimization results are presented and discussed in the following sections.

OPTIMAL STRENGTH DESIGN

There are two optimization methods [26] provided by ANSYS namely, subproblem approximation method and first-order method. Subproblem approximation method requires only the value of the dependent variables (objective function and constraint function), which are approximated by means of least squares fitting. The first-order method uses gradients of the dependant variables. In each iteration, using a steepest descent or conjugate direction method, a search direction is selected and the unconstrained minimization problem is solved along the specified direction. As is expected, each iteration consists of a large number of subiterations calculating search directions as well as gradients. Hence, the first-order method for optimization performs requires substantially longer CPU time in comparison to that required by the subproblem method.

The subproblem approximation method, due to its independency from using derivatives of the problem variables and efficiency of CPU time, is the first candidate used in the optimization subroutine. It can be efficiently applied to most engineering problems [27–32]. However, it is found [27] that for subproblem approximation method the solution is sensitive to the initial designs. If an unsuitable initial design set is given, the solution will be far from the global optimum solution. In order to overcome this disadvantage, a technique of applying an evolution-based optimization algorithm PSO integrated with ANSYS was developed for optimization in this study.

Particle Swarm Optimization

PSO was basically developed through simulation of bird flocking in 2D space [33]. The PSO algorithm is based on a simplified social model and it mimics the behavior of a bird flock in search for food. This so-called evolution-based algorithm does not require continuity and derivative existence of the objective function or constraint function. It is robust and can provide a more reliable approach to obtain the global optimum in nonsmooth or nonlinear problems as compared to the gradient-based methods. While it does not guarantee an optimal point, it is capable of finding the global minima due to their ability to jump across the whole design space. It is a population-based search algorithm, where each individual is referred to as a particle and represents a candidate solution. To discover the optimal solution, each particle changes its searching direction according to two factors, its own best previous experience (pBest) and the best experience of all other members (gBest). Every swarm continuously updates itself through the above-mentioned best solutions. Thus, a new generation of community comes into being, which has moved closer toward the best solution, ultimately converging onto the optimal solution. In practical operation, one assesses which particle is better through the fitness function, which is determined by the optimization objective. Let the i-th particle denote a point in the $\boldsymbol{D}$ dimensional space. The position of the i-th particle is expressed as $X_i = (x_{i1}, x_{i2}, \ldots, x_{iD})^{\mathrm{T}}$ and the velocity is expressed as $V_i = (v_{i1}, v_{i2}, \ldots, v_{iD})^{\mathrm{T}}$. The particles are renewed according to the following Equations (16) and (17).

$$v_{id}^{k+1} = \chi \times [w v_{id}^{k} + c_1 \mathrm{rand}_1^k()(pBest_{id}^k - x_{id}^k) + c_2 \mathrm{rand}_2^k()(gBest_{id}^k - x_{id}^k)], \tag{16}$$

$$x_{id}^{k+1} = x_{id}^{k} + v_{id}^{k+1}, \tag{17}$$

where the subscript i denotes the particle and the superscript k the iteration number; $\text{rand}_1^k()$ and $\text{rand}_2^k()$ are the random numbers uniformly distributed in the range [0,1]; c_1 and c_2 the acceleration constants, both taking the values around two in general cases; w the inertia weight parameter [34] and χ the constriction factor [35] which may help to ensure convergence. Other improvements of PSO can be found in our previous study [36].

Optimization Procedure Combining PSO and FEM

The optimization procedure is essentially written in MATLAB. In the optimization process, the procedure first initializes the swarm. ANSYS is then called on the back stage to evaluate the objective and constraint functions of each particle through the APDL commands written beforehand. ANSYS outputs the values of the functions to an external file. MATLAB reads them and computes the penalty function as fitness of each particle. Every particle updates itself through Equations (16) and (17). The updated swarm is then returned to ANSYS for the next iteration. This process is repeated until the number of iteration reaches the pre-determined maximum iteration number. In the whole optimization process, data from ANSYS and MATLAB are exchanged back and forth with each other, as shown in Figure 9. Based on this procedure, we can use other FE codes to substitute for ANSYS and other evolution-based optimization algorithms such as genetic algorithm (GA) to substitute for PSO. The advantage of PSO over GA is that PSO does not need complicated encoding, decoding, or special genetic operators such as mutation and crossover. So PSO has fewer parameters to be adjusted. It is therefore more effective in terms of CPU time [28]. The number of ANSYS invoked equals to the number of maximum iteration number multiplied by the number of particles. For PSO, the typical range for the number of particles is 20–40. For most of problems, 10 particles are large enough to get good results. In this study, a particle size of 15 is chosen. The maximum number of iterations is assigned to be 15, since the improvement in the objective function after 15 iterations is negligible.

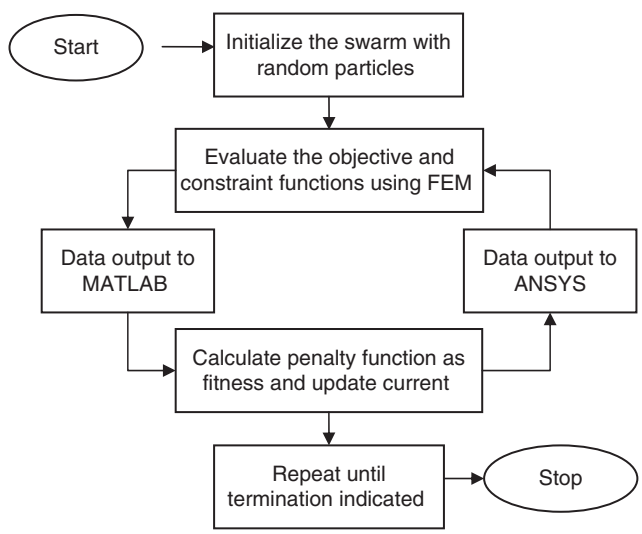

Figure 9. *Flow chart of optimization process.*

Optimal Strength Design Formulation

In the finite element analysis (FEA) of the laminated composites, if N is the number of elements in an individual layer, nf the number of FRP layers and nm the number of metal layers, the fitness function (FI) is calculated at each element and among these finesses, the maximum fitness is sought and minimized with respect to the ply orientation of FRP layers θ. The ply angle of metal layer can be neglected as the metal layer is isotropic. The problem is described as follows:

$$\begin{aligned}\text{Minimize } & \max_{\theta}\begin{bmatrix} f_1^1(\theta_\mathrm{f}), f_1^2(\theta_\mathrm{f}), \ldots, f_1^N(\theta_\mathrm{f}) \\ f_2^1(\theta_\mathrm{f}), f_2^2(\theta_\mathrm{f}), \ldots, f_2^N(\theta_\mathrm{f}) \\ \vdots \\ f_{nf}^1(\theta_\mathrm{f}), f_{nf}^2(\theta_\mathrm{f}), \ldots, f_{nf}^N(\theta_\mathrm{f}) \\ f_1^1(\theta_\mathrm{m}), f_1^2(\theta_\mathrm{m}), \ldots, f_1^N(\theta_\mathrm{m}) \\ f_2^1(\theta_\mathrm{m}), f_2^2(\theta_\mathrm{m}), \ldots, f_2^N(\theta_\mathrm{m}) \\ \vdots \\ f_{\mathrm{nm}}^1(\theta_\mathrm{m}), f_{\mathrm{nm}}^2(\theta_\mathrm{m}), \ldots, f_{\mathrm{nm}}^N(\theta_\mathrm{m}) \end{bmatrix}, \\ \text{Subject to } & -90^\circ \le \theta \le 90^\circ \end{aligned} \tag{18}$$

where, $f_i^j(\theta_f)$, $f_i^j(\theta_m)$ are respectively the failure indices of the j-th element in the i-th FRP layer or the i-th metal layer.

In-plane loads consider uniaxial and biaxial tensile loads (Figure 10). Uniaxial load is $N_x = 500\,\mathrm{N/mm}$. Biaxial loads have two cases: $N_x = 100\,\mathrm{N/mm}$ and $N_y = 200\,\mathrm{N/mm}$; $N_x = 150\,\mathrm{N/mm}$ and $N_y = 150\,\mathrm{N/mm}$. The former case can simulate the stress state in a cylindrical pressure vessel under internal pressure load condition. A out-of-plane point force was applied at the center of a laminate as shown in Figure 11.

The applied point load is $Pz = 0.25\,\mathrm{kN}$. All the loads are applied monotonously. For out-of-plane load, four boundary conditions as shown in Figure 12 are considered: (1) all edges are fixed, (2) all edges are simply supported, (3) two edges are fixed and the other two are simply supported, and (4) two edges are fixed, the other two are free.

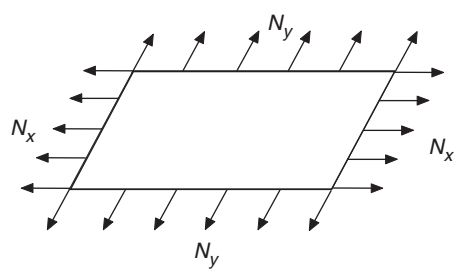

Figure 10. *In-plane load.*

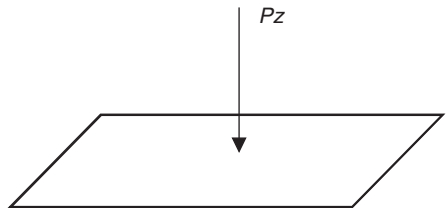

Figure 11. *Out-of-plane load.*

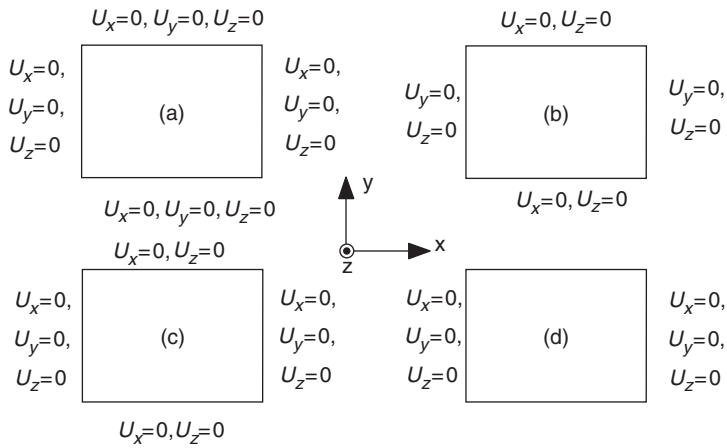

Figure 12. *Boundary conditions under point load.*

Optimization Results and Discussion

The material of FRP is T300/epoxy, stacking as $[\alpha/\theta/\beta/\alpha/\beta/\theta/\alpha]$ with α, θ, and β being design variables. In order to compare the strength behavior of FML and FRP, we substituted the α layer with aluminum sheet to form FML: [Al/θ/β/Al/β/θ/Al]. FML and FRP are of the same dimensions $100 \times 100\,\text{mm}^2$, and the thickness is 0.2 mm for each layer. Al2024-T3 and Al7075-T6 are two types of aluminum alloy widely used in FML. FML with 2024-T3 and 7075-T6 is denoted as FML-T3 and FML-T6, respectively. The material properties of FRP [37] and aluminum sheet [38] are listed in Table 4.

The same mesh is used for FRP and FML. As mentioned earlier, the mesh is denser at the free edge for in-plane load conditions. For out-of-plane load, the mesh is denser at the center of the laminated plate as the stresses are concentrating there. It is well-known that the calculated stress value by FE code depends upon the denseness of the FE mesh. With a denser mesh, a quantitatively more precise analysis of the objective function value can be obtained. Thus, the mesh is crucial. In order to have an insight into the mesh to chose, a study of mesh sensitivity on the calculated FI was conducted for biaxial load and point load, respectively, for a sampled laminate as shown in Figure 13.

It is observed that for in-plane load, meshes have weak impact on FI and the mesh $5 \times 15 \times 7$ gives FI close to others with least computational effort; thus, it is chosen for the optimization calculation. For out-of-plane load, the meshes have somewhat a good effect

Table 4. Material properties for optimization.

Properties	FRP (T300/epoxy)	Properties	Al2024-T3	Al7075-T6
E_1(GPa)	135	E_e (GPa)	71	72
$E_2 = E_3$ (GPa)	10	E_p (MPa)	744.7	631.1
$G_{12} = G_{13}$ (GPa)	5.0	–	–	–
G_{23} (GPa)	3.972	–	–	–
$\mu_{12} = \mu_{23} = \mu_{13}$	0.27	μ	0.33	0.33
X_t, X_C (MPa)	1459, 1400	ε_{ult} (%)	15.9	11
Y_t, Y_C (MPa)	55,170	σ_y (MPa)	381	505
$R = S = T$ (MPa)	90	σ_{ult} (MPa)	496.2	570
ρ (kg/mm^3)	1.54E−6	ρ (kg/mm^3)	2.72E−6	2.82E−6

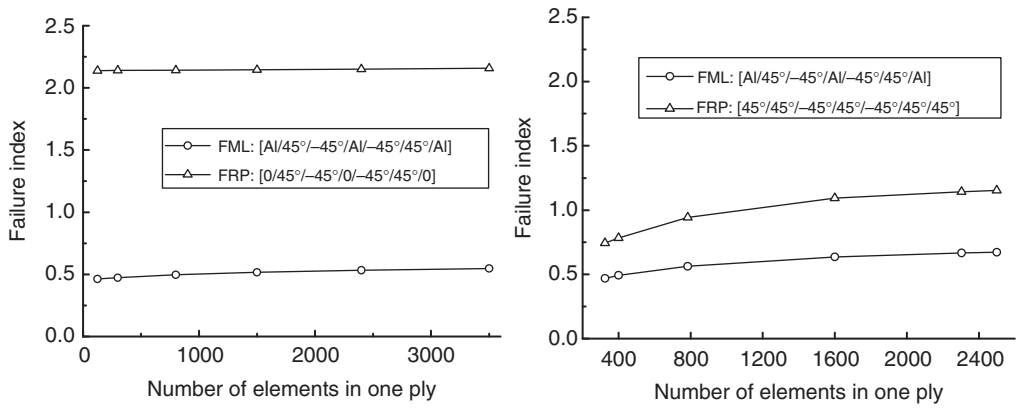

Figure 13. *Mesh effect on the calculated FI for biaxial load ($N_x = 150$ N/mm, $N_y = 150$ N/mm, left) and point load (right).*

on FI; the denser the mesh, the larger the FI and the subsequent increase in the FI with the increase in the number of elements is relatively slow. For optimization problems, the difference of alternative candidates is the concern. Consequently, a sparse mesh of $20 \times 20 \times 7$ is used to save the computational effort.

The optimization results for in-plane load are given in Table 5 and the optimization results for out-of-plane load are given in Table 6. In order to have visualized presentation of the optimization results, an illustration was shown in Figure 14.

For in-plane uniaxial load, the optimum FI of FML and FRP occurs when all the fiber angles are near 0° and the worst FI occurs when the fiber angles are near 90°. The fiber angles are close to 0° or 90°, but not exactly these values. This is due to the characteristic of the evolution nature of the optimization algorithm. The optimum FI of FRP is lower than FML, as the longitudinal tensile strength of a lamina is greater than the yielding strength of Al. The worst FI of FRP is greater than FML, as the transverse tensile strength of a lamina is much lower than the yielding strength of Al. It demonstrates that the substituting of aluminum alloy sheet for prepreg layer enhances the strength behavior of transverse direction. For biaxial load, although the FRP laminate has more optimizing flexibility (three design variables for each layer), the optimum FI of FML is lower than FRP, and the

Table 5. Optimization results for in-plane load.

Load (N/mm)	Material	Optimum angle	Optimum FI	Worst angle	Worst FI
$N_x = 500$, $N_y = 0$	FRP	$[0.5/-0.05/0.3/0.5_{1/2}]s$	0.055	$[90.6/87.3/82.8/90.6_{1/2}]s$	18.06
	FML-T3	$[Al/-0.3/-0.4/Al_{1/2}]s$	0.65	$[Al/-89.7/79.6/Al_{1/2}]s$	12.8
	FML-T6	$[Al/1.2/-0.3/Al_{1/2}]s$	0.49	$[Al/71.7/89.4/Al_{1/2}]s$	7.31
$N_x = 100$, $N_y = 200$	FRP	$[73.4/78.1/-22.3/73.4_{1/2}]s$	0.63	$[-0.7/-7.8/64.6/-0.7_{1/2}]s$	4.14
	FML-T3	$[Al/84.2/-82.7/Al_{1/2}]s$	0.38	$[Al/1.7/1/Al_{1/2}]s$	2.64
	FML-T6	$[Al/-88.3/84.4/Al_{1/2}]s$	0.29	$[Al/-0.8/-0.8/Al_{1/2}]s$	2.63
$N_x = 150$, $N_y = 150$	FRP	$[79.9/-2.9/-84.5/79.9_{1/2}]s$	0.55	$[-38.7/-84/-36/-38.7_{1/2}]s$	2.96
	FML-T3	$[Al/41.4/-66.2/Al_{1/2}]s$	0.41	$[Al/0.03/5.8/Al_{1/2}]s$	1.75
	FML-T6	$[Al/-51.9/59.2/Al_{1/2}]s$	0.38	$[Al/4.6/3.9/Al_{1/2}]s$	1.74

Table 6. Optimization results for out-of plane load.

BC	Material	Optimum angle	Optimum FI	Worst angle	Worst FI
a	FRP	$[-86.8/10.5/-8.4/-86.8_{1/2}]s$	0.75	$[44.6/43.2/41.3/44.6_{1/2}]s$	2.59
	FML-T3	$[Al/-34.2/81.7/Al_{1/2}]s$	0.65	$[Al/-44.5/-36.6/Al_{1/2}]s$	0.68
	FML-T6	$[Al/82.1/-11/Al_{1/2}]s$	0.49	$[Al/39.0/38.5/Al_{1/2}]s$	0.51
b	FRP	$[41.4/-48.4/-46.5/41.4_{1/2}]s$	0.91	$[29.4/28.6/28.8/29.4_{1/2}]s$	2.96
	FML-T3	$[Al/-45.8/49.5/Al_{1/2}]s$	0.75	$[Al/-84.6/-85.2/Al_{1/2}]s$	0.79
	FML-T6	$[Al/38.9/-46.6/Al_{1/2}]$	0.56	$[Al/-9.8/-4.1/Al_{1/2}]s$	0.60
c	FRP	$[1.2/-84.3/80.2/1.2_{1/2}]s$	0.73	$[-66/-66.8/-67.8/-66_{1/2}]s$	2.92
	FML-T3	$[Al/9.1/-59.4/Al_{1/2}]s$	0.66	$[Al/79.2/80.3/Al_{1/2}]s$	0.73
	FML-T6	$[Al/11/-64.2/Al_{1/2}]$	0.50	$[Al/88.4/-85.9/Al_{1/2}]s$	0.55
d	FRP	$[-2.3/86/76.4/-2.3_{1/2}]s$	0.74	$[-80.9/-83/-79.1/-80.9_{1/2}]s$	3.93
	FML-T3	$[Al/-1.2/87/Al_{1/2}]s$	0.65	$[Al/75.4/69.9/Al_{1/2}]s$	0.73
	FML-T6	$[Al/-11.5/61.7/Al_{1/2}]s$	0.49	$[Al/64.9/-26.9/Al_{1/2}]s$	0.55

Note: BC, boundary condition.

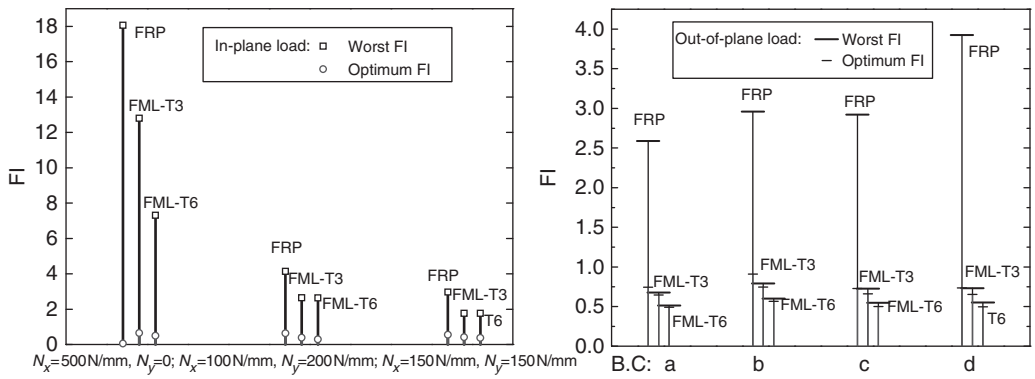

Figure 14. *Schematic illustration of the optimization results under in-plane load and point load.*

worst FI of FML is also lower than FRP. It indicates that due to the enhancement in the transverse direction, FML exhibits superior strength performance to that offered by FRP under biaxial load. In addition, it is observed that when the load changes from uniaxial to biaxial, the optimum FI of FRP rises from 0.055 to 0.63 or 0.55, respectively. In contrast,

the optimum FI of FML-T3 descends from 0.65 to 0.38 or 0.41 and that of FML-T6 descends from 0.49 to 0.29 or 0.38. It is concluded that comparing with FRP, FML is of better capability to withstand biaxial load. As the yielding strength of Al7075-T6 is greater than Al2024-T3, the optimum and the worst FI of FML-T6 are lower than FML-T3.

Under point load conditions, for all the boundary conditions in Figure 12, the optimum FI of FML-T3 and FML-T6 are all lower than FRP, and the worst FI are also lower than FRP. All the worst FI of FML are found to be lower than 1, implying that under the point load of $Pz = 0.25$ kN, whatever the value the fiber angles take in the design space, FML-T3 and FML-T6 will not fail. In addition, it can be observed that the ratio of the worst FI vs. the optimum one of FML-T3 and FML-T6 was much smaller than FRP. It indicates that under out-of-plane load, FML exhibits superior strength behavior than FRP and at the same time, the strength behavior is much more stable than FRP laminates.

In this article, the optimization equation can be more than just strength, also fatigue, damage tolerance, design costs, and qualification issues, etc. These equations can be specified as design objective or constraint objective with the proposed optimization method, as for PSO the dynamic penalty function method can be used to deal with a constrained optimization problem conveniently [36]. These objective functions or constraint functions are evaluated by FEA for different load cases.

In practice, the thickness of laminate is prone to be a design variable and we have done some study to optimize the total weight of laminates by tailoring the layer thickness in our previous study. In this article, we aimed to optimize the strength and compare the optimal strength of FRP and FML, rather than the weight of laminate. Therefore, the 'optimal strength' in this article can be regarded as 'idealized optimal strength,' since that the layer thickness as variable is not yet considered. For some practical engineering optimization problems, design variables may behave as discrete ones for manufacturing reasons. For example, the thickness of a ply is defined as a set of discrete values [0.1 mm, 0.2 mm, 0.3 mm...] and the fiber orientations of the plies are limited to [0, 15°, 30°, 45°...]. This greatly reduces the design space. In some cases, we can convert the optimum values of continuous results to the nearest discrete manufacturable values. And for some other problems, the discrete optimization problems can be directly solved with PSO by using a specially coding technology as done in our previous study [36]. Hence, it is expected that the proposed methodology is applicable to dealing with engineering problems with continuous, discrete, or the mixed variables.

CONCLUSIONS

Nowadays, besides the existing products of FML, some new types of FML consisting of other constituents are under development. It is expected that the application of FML in aerospace/aeronautical structures will be further enhanced. This article presents a methodology that combines PSO with the FE code ANSYS for the optimum design of FML or FRP. The failure indices of FML or FRP are taken to be the objective and the fiber angles are design variables. The optimization results demonstrate that: (1) owing to the substituting of metal alloy sheet for prepreg layer, the strength behavior in transverse direction was enhanced; (2) FML exhibits superior strength behavior than FRP under biaxial load. Comparing with FRP, FML is of better capability to withstand biaxial load; (3) FML exhibits superior strength behavior than FRP and is more stable under out-of-plane load; (4) This article also modified and extended CLT to make it applicable for FML. This gives

a foundation for the reliability analysis and evaluation of elastic or elastic–plastic properties of FML.

By merging the general FE package and evolution-based optimization algorithm with parallel computing scheme, it is believed that the proposed approach provides designers a feasible and efficient methodology with a great potential in developing the tailoring applications in composite structural design and other complex engineering designs.

ACKNOWLEDGMENTS

This study was supported by the Natural Sciences Foundation of China (no. 10772070), PhD Programs Foundation of Ministry of Education of China (no. 20070487064), and the Open Project of State Key Lab. of Structural Analysis for Industrial Equipment (no. GZ0810). These supports are acknowledged gratefully.

REFERENCES

1. Vlot, A. (1996). Impact Loading on Fibre Metal Laminates, *Int. J. Impact Eng.*, **18**(3): 291–307.
2. Caprino, G., Spataro, G. and Del Luongo, S. (2004). Low-velocity Impact Behavior of Fibreglass-Aluminium Laminates, *Composites Part A*, **35**: 605–616.
3. Khalili, S.M.R., Mittal, R.K. and Gharibi Kalibar, S. (2005). A Study of the Mechanical Properties of Steel/Aluminium/GRP Laminates, *Mater. Sci. Eng., A*, **412**: 137–140.
4. Vogelesang, L.B. and Vlot, A. (2000). Development of Fibre Metal Laminates for Advanced Aerospace Structures, *J. Mater. Process. Technol.*, **103**: 1–5.
5. Vermeeren, C.A.J.R., Beumler, Th., de Kanter, J.L.C.G., van der Jagt, O.C. and Out, B.C.L. (2003). GLARE Design Aspects and Philosophies, *Appl. Compos. Mater.*, **10**: 257–276.
6. Afaghi-Khatibi, A., Lawcock, G., Ye, L. and Mai, Y.-W. (2000). On the Fracture Mechanical Behaviour of Fibre Reinforced Metal Laminates (FRMLs), *Comput. Meth. Appl. Mech. Eng.*, **185**: 173–190.
7. Davisaon, D.L. and Austin, L.K. (1991). Fatigue Crack Growth through ARALL-4 at Ambient Temperature, *Fatigue Fract. Eng. Mater. Struct.*, **14**: 939–951.
8. Sinke, J. (2003). Manufacturing of GLARE Parts and Structrues, *Appl. Compos. Mater.*, **10**: 293–305.
9. Kawai, M., Morishita, M., Tomura, S. and Takumida, K. (1998). Inelastic Behaviour and Strength of Fiber–Metal Hybrid Composite: GLARE, *Int. J. Mech. Sci.*, **40**: 183–198.
10. Kim, J.S. (2007). Development of a User-Friendly Expert System for Composite Laminate Design, *Compos. Struct.*, **79**: 76–83.
11. Park, J.H., Hwang, J.H., Lee, C.S. and Hwang, W. (2001). Stacking Sequence Design of Composite Laminates for Maximum Strength Using Genetic Algorithms, *Compos. Struct.*, **52**(2): 217–231.
12. Walker, M. and Smith, R.E. (2003). A Technique for the Multi-objective Optimization of Laminated Composite Structures Using Genetic Algorithms and Finite Element Analysis, *Compos. Struct.*, **62**(1): 123–128.
13. Barakat, S.A. and Abu-Farsak, G.A. (1999). The Use of an Energy-based Criterion to Determine Optimum Configurations of Fibrous Composites, *Compos. Sci. Technol.*, **59**: 1891–1899.
14. Omkar, S.N., Dheevatsa Mudigere, G., Narayana Naik, G. and Gopalakrishnan, S. (2008). Vector Evaluated Particle Swarm Optimization (VEPSO) for Multi-objective Design Optimization of Composite Structure, *Comput. Struct.*, **86**: 1–14.
15. Akbulut, M. and Sonmez, F.O. (2008). Optimum Design of Composite Laminates for Minimum Thickness, *Compos. Struct.*, **86**(21–22): 1974–1982.

16. Narayana Naik, G., Gopalakrishnan, S. and Ganguli, R. (2008). Design Optimization of Composites Using Genetic Algorithms and Failure Mechanism Based Failure Criterion, *Compos. Struct.*, **83**: 354–367.
17. Pelletier, J.L. and Vel, S.S (2006). Multi-objective Optimization of Fiber Reinforced Composite Laminates for Strength, Stiffness and Minimal Mass, *Comput. Struct.*, **84**: 2065–2080.
18. Edgar Fuossa, P.V. (1998). Effects of Stacking Sequence on the Impact Resistance Laminates-Part 1: Parametric Study in Composite, *Compos. Struct.*, **41**: 67–77.
19. Sun, C.T. and Jih, C.J. (1995). Quasi-static Modeling of Delamination Crack Propagation in Laminates Subjected to Low-velocity Impact, *Compos. Sci. Technol.*, **54**: 185–191.
20. de Moura, M.F.S.F. and Marques, A.T. (2002). Prediction of Low Velocity Impact Damage in Carbon–Epoxy Laminates, *Composites Part A*, **33**: 361–368.
21. Jones, R.M. (1998). *Mechanics of Composite Materials*, **2nd edn**, Taylor and Francis Publ, Philadelphia.
22. Wu, G. and Yang, J.-M. (2005). Analytical Modelling and Numerical Simulation of the Nonlinear Deformation of Hybrid Fibre–Metal Laminates, *Modell. Simul. Mater. Sci. Eng.*, **13**: 413–425.
23. Tsai, W. (1988). *Composites Design*, **4th edn**, Think composite, Dayton, OH, USA.
24. Pipes, R.B. and Cole, B.W. (1973). On the Off-axis Strength Test for Anisotropic Composite Laminate, *J. Compos. Mater.*, **7**: 246–256.
25. Cortes, P. and Cantwell, W.J. (2006). The Prediction of Tensile Failure in Titanium-based Thermoplastic Fibre-metal Laminate, *Compos. Sci. Technol.*, **66**: 2306–2316.
26. ANSYS (2003). *ANSYS Theory Reference Manual*, Release 8.0, Ansys Inc, Canonsburg, PA, USA.
27. Chen, J.Q., Peng, W.J., Ge, R. and Wei, J.H. (2009). Optimal Design of Composite Laminates for Minimizing Delamination Stresses by Particle Swarm Optimization Combined with FEM, *Struct. Eng. Mech.*, **31**(4): 407–421.
28. Hassan, R., Cohanim, B.K, Weck, O.D. and Venter, G. (2005). A Comparison of Particle Swarm Optimization and the Genetic Algorithm, In: *Proceedings of the 46th AIAA/ASME/ASCE/AHS/ASC Structures, Structural Dynamics and Materials Conference*, Austin, TX.
29. Kayabasi, O. and Ekici, B. (2007). The Effects of Static, Dynamic and Fatigue Behavior on Three-dimensional Shape Optimization of Hip Prosthesis by Finite Element Method, *Mater. Des.*, **28**: 2269–2277.
30. Kurtaran, H., Buyuk, M. and Eskandarian, A. (2003). Design Automation of a Laminated Armor for Best Impact Performance Using Approximate Optimization Method, *Int. J. Impact. Eng.*, **29**: 397–406.
31. Bayandor, J., Scott, M.L. and Thomson, R.S. (2002). Parametric Optimisation of Composite Shell Structures for an Aircraft Krueger Flap, *Compos. Struct.*, **57**: 415–423.
32. Hossain, M.M., Jagarkal, S.G., Agonafer, D., Lulu, M. and Reh, S. (2007). Design Optimization and Reliability of PWB Level Electronic Package, *J. Electron. Packag.*, **129**: 9–18.
33. Kennedy, J. and Eberhart, R.C. (1995). Particle Swarm Optimization, In: *Proceedings of the 1995 IEEE International Conference Neural Networks*, Perth, Australia, IEEE Service Center, Piscataway, NJ, pp. 1942–1948.
34. Shi, Y.H. and Eberhart, R. (1998). Parameter Selection in Particle Swarm Optimization, In: *Evolutionary Programming VII, Lecture Notes Computer Science*, pp. 591–600.
35. Clerc, M. (1999). The Swarm and the Queen: Towards a Deterministic and Adaptive Particle Swarm Optimization, In: *Proceedings of the 1999 Congress on Evolutionary Computation*, Washington DC, USA, IEEE Service Center, Piscataway, NJ, pp. 1951–1957.
36. Chen, J.Q., Ge, R. and Wei, J.H. (2008). Probabilistic Optimal Design of Laminates by Using the Improved Particle Swarm Optimization, *Eng. Optim.*, **40**(8): 695–708.
37. Lindemann, J. and Becker, W. (2002). The Tendency for Free-edge Delamination in Laminates and its Minimization, *Compos. Sci. Technol.*, **62**: 233–242.
38. Iaccarino, P., Langella, A. and Caprino, G. (2007). A Simplified Model to Predict the Tensile and Shear Stress–Strain Behaviour of Fibreglass/Aluminium Laminates, *Compos. Sci. Technol.*, **67**: 1784–1793.